

QCD Coulomb Gauge Approach to Exotic Hadrons

Stephen R. Cotanch, Ignacio J. General and Ping Wang

Department of Physics, North Carolina State University, Raleigh NC 27695-8202 USA

Received: date / Revised version: date

Abstract. The Coulomb gauge Hamiltonian model is used to calculate masses for selected J^{PC} states consisting of exotic combinations of quarks and gluons: ggg glueballs (oddballs), $q\bar{q}g$ hybrid mesons and $q\bar{q}q\bar{q}$ tetraquark systems. An odderon Regge trajectory is computed for the J^{--} glueballs with intercept much smaller than the pomeron, explaining its nonobservation. The lowest 1^{-+} hybrid meson mass is found to be just above 2.2 GeV while the lightest tetraquark state mass with these exotic quantum numbers is predicted around 1.4 GeV consistent with the observed $\pi(1400)$.

PACS. 12.38.Lg Other nonperturbative calculations – 12.39.Ki Relativistic quark model – 12.39.Mk Glueball and nonstandard multi-quark/gluon states – 12.40.Yx Hadron mass models and calculations

1 Introduction

Establishing the existence of exotic hadrons (non $q\bar{q}$ or qqq structure) is of paramount importance and remains one of the key unsolved problems in hadronic physics. In particular, it is expected from general QCD principles that nonconventional color singlet states of gluons and quarks should exist such as glueballs (gg and ggg), hybrid mesons ($q\bar{q}g$) and multi-quark states ($q\bar{q}q\bar{q}$ and $qqqq\bar{q}\bar{q}$). The present work addresses the structure of these hadrons and provides new information to assist experimental searches.

2 Coulomb Gauge Hamiltonian Model

In a series of publications [1, 2, 3, 4, 5, 6, 7, 8] a realistic model for hadron structure has been developed and applied to the quark and gluon sectors. This field theoretical, relativistic many-body approach utilizes an effective QCD Hamiltonian, H_{eff} , formulated in the Coulomb gauge. It properly incorporates chiral symmetry using standard bare current quark masses but dynamically generates a constituent mass and spontaneous chiral symmetry breaking [2]. Through approximate many-body diagonalizations it successfully describes the meson spectrum [4, 6] and is consistent [7] with lattice glueball predictions. It also yields a good description of the vacuum properties (quark and gluon condensates) within a minimal two parameter theory.

The effective Hamiltonian, an approximation to the exact Coulomb gauge QCD Hamiltonian, is

$$H_{\text{eff}} = H_q + H_g + H_{qg} + H_C \quad (1)$$

$$H_q = \int d\mathbf{x} \Psi^\dagger(\mathbf{x}) [-i\boldsymbol{\alpha} \cdot \boldsymbol{\nabla} + \beta m] \Psi(\mathbf{x}) \quad (2)$$

$$H_g = \frac{1}{2} \int d\mathbf{x} [\boldsymbol{\Pi}^a(\mathbf{x}) \cdot \boldsymbol{\Pi}^a(\mathbf{x}) + \mathbf{B}^a(\mathbf{x}) \cdot \mathbf{B}^a(\mathbf{x})] \quad (3)$$

$$H_{qg} = g \int d\mathbf{x} \mathbf{J}^a(\mathbf{x}) \cdot \mathbf{A}^a(\mathbf{x}) \quad (4)$$

$$H_C = -\frac{1}{2} \int d\mathbf{x} d\mathbf{y} \rho^a(\mathbf{x}) \hat{V}(|\mathbf{x} - \mathbf{y}|) \rho^a(\mathbf{y}) , \quad (5)$$

with g the QCD coupling, Ψ the quark field, m the current quark mass, \mathbf{A}^a the gluon fields satisfying the transverse gauge condition, $\boldsymbol{\nabla} \cdot \mathbf{A}^a = 0$, $a = 1, 2, \dots, 8$, $\boldsymbol{\Pi}^a$ the conjugate fields and \mathbf{B}^a the non-abelian magnetic fields

$$\mathbf{B}^a = \boldsymbol{\nabla} \times \mathbf{A}^a + \frac{1}{2} g f^{abc} \mathbf{A}^b \times \mathbf{A}^c . \quad (6)$$

The color densities, $\rho^a(\mathbf{x})$, and currents, \mathbf{J}^a , are

$$\rho^a(\mathbf{x}) = \Psi^\dagger(\mathbf{x}) T^a \Psi(\mathbf{x}) + f^{abc} \mathbf{A}^b(\mathbf{x}) \cdot \boldsymbol{\Pi}^c(\mathbf{x}) \quad (7)$$

$$\mathbf{J}^a = \Psi^\dagger(\mathbf{x}) \boldsymbol{\alpha} T^a \Psi(\mathbf{x}) , \quad (8)$$

with $T^a = \frac{\lambda^a}{2}$ and f^{abc} the SU_3 color matrices and structure constants, respectively. Confinement is described by a Cornell type potential,

$$\hat{V}(r = |\mathbf{x} - \mathbf{y}|) = \hat{V}_C(r) + \hat{V}_L(r) \quad (9)$$

$$\hat{V}_C(r) = -\frac{\alpha_s}{r} \quad (10)$$

$$\hat{V}_L(r) = \sigma r , \quad (11)$$

with previously determined string tension, $\sigma = 0.135 \text{ GeV}^2$, and $\alpha_s = \frac{g^2}{4\pi} = 0.4$. Below we denote the Fourier transform of \hat{V} by V .

The bare fields have the Fock operator expansions (quark spinors u, v , helicity, $\lambda = \pm 1$, and color vectors $\hat{e}_{C=1,2,3}$)

$$\Psi(\mathbf{x}) = \int \frac{d\mathbf{k}}{(2\pi)^3} \psi_C(\mathbf{k}) e^{i\mathbf{k} \cdot \mathbf{x}} \hat{e}_C \quad (12)$$

$$\Psi_C(\mathbf{k}) = u_\lambda(\mathbf{k})b_{\lambda C}(\mathbf{k}) + v_\lambda(-\mathbf{k})d_{\lambda C}^\dagger(-\mathbf{k}) \quad (13)$$

$$\mathbf{A}^a(\mathbf{x}) = \int \frac{d\mathbf{k}}{(2\pi)^3} \frac{1}{\sqrt{2k}} [\mathbf{a}^a(\mathbf{k}) + \mathbf{a}^{a\dagger}(-\mathbf{k})] e^{i\mathbf{k}\cdot\mathbf{x}} \quad (14)$$

$$\Pi^a(\mathbf{x}) = -i \int \frac{d\mathbf{k}}{(2\pi)^3} \sqrt{\frac{k}{2}} [\mathbf{a}^a(\mathbf{k}) - \mathbf{a}^{a\dagger}(-\mathbf{k})] e^{i\mathbf{k}\cdot\mathbf{x}}, \quad (15)$$

with quark, anti-quark and gluon Fock operators $b_{\lambda C}(\mathbf{k})$, $d_{\lambda C}(-\mathbf{k})$ and $a_\mu^a(\mathbf{k})$ ($\mu = 0, \pm 1$), respectively. The Coulomb gauge condition, $\mathbf{k} \cdot \mathbf{a}^a(\mathbf{k}) = (-1)^\mu k_\mu a_{-\mu}^a(\mathbf{k}) = 0$, produces transverse commutation relations,

$$[a_\mu^a(\mathbf{k}), a_{\mu'}^{b\dagger}(\mathbf{k}')] = (2\pi)^3 \delta_{ab} \delta^3(\mathbf{k} - \mathbf{k}') D_{\mu\mu'}(\mathbf{k}), \quad (16)$$

with

$$D_{\mu\mu'}(\mathbf{k}) = \delta_{\mu\mu'} - (-1)^\mu \frac{k_\mu k_{-\mu'}}{k^2}. \quad (17)$$

The ground state (model vacuum) is generated using the Bardeen-Cooper-Schrieffer (BCS) method, entailing rotated field operators (Bogoliubov-Valatin transformation),

$$\begin{aligned} B_{\lambda C}(\mathbf{k}) &= \cos \frac{\theta_k}{2} b_{\lambda C}(\mathbf{k}) - \lambda \sin \frac{\theta_k}{2} d_{\lambda C}^\dagger(-\mathbf{k}) \\ D_{\lambda C}(-\mathbf{k}) &= \cos \frac{\theta_k}{2} d_{\lambda C}(-\mathbf{k}) + \lambda \sin \frac{\theta_k}{2} b_{\lambda C}^\dagger(\mathbf{k}) \\ \alpha^a(\mathbf{k}) &= \cosh \theta_k a^a(\mathbf{k}) + \sinh \theta_k a^{a\dagger}(-\mathbf{k}), \end{aligned} \quad (18)$$

producing the dressed, quasi-particle operators α^a , $B_{\lambda C}$ and $D_{\lambda C}$, respectively. The quasi-particle (BCS) vacuum, determined by $B_{\lambda C}|\Omega\rangle = D_{\lambda C}|\Omega\rangle = \alpha_\mu^a|\Omega\rangle = 0$, is built on the bare parton one, $b_{\lambda C}|0\rangle = d_{\lambda C}|0\rangle = a_\mu^a|0\rangle = 0$,

$$|\Omega_{quark}\rangle = e^{-\int \frac{d\mathbf{k}}{(2\pi)^3} \lambda \tanh \frac{\theta_k}{2} b_{\lambda C}^\dagger(\mathbf{k}) d_{\lambda C}^\dagger(-\mathbf{k})} |0\rangle \quad (19)$$

$$|\Omega_{gluon}\rangle = e^{-\int \frac{d\mathbf{k}}{(2\pi)^3} \frac{1}{2} \tanh \theta_k D_{\mu\mu'}(\mathbf{k}) a_\mu^{a\dagger}(\mathbf{k}) a_{\mu'}^{a\dagger}(-\mathbf{k})} |0\rangle. \quad (20)$$

The composite BCS vacuum, $|\Omega\rangle = |\Omega_{quark}\rangle \otimes |\Omega_{gluon}\rangle$, contains quark and gluon condensates (correlated $q\bar{q}$ and gg Cooper pairs). A variational minimization of the vacuum expectation value of the Hamiltonian, $\delta\langle\Omega|H_{\text{eff}}|\Omega\rangle = 0$, yields the constituent quark and gluon gap equations

$$ks_k - mc_k = \frac{2}{3} \int \frac{d\mathbf{q}}{(2\pi)^3} (s_k c_q x - s_q c_k) V(|\mathbf{k} - \mathbf{q}|) \quad (21)$$

$$\begin{aligned} \omega_k^2 &= k^2 - \frac{3}{4} \int \frac{d\mathbf{q}}{(2\pi)^3} V(|\mathbf{k} - \mathbf{q}|) [1 + x^2] \left(\frac{\omega_q^2 - \omega_k^2}{\omega_q} \right) \\ &+ \frac{3}{4} g^2 \int \frac{d\mathbf{q}}{(2\pi)^3} \frac{1 - x^2}{\omega_q}, \end{aligned} \quad (22)$$

with $s_k = \sin\phi_k$, $c_k = \cos\phi_k$ and $x = \mathbf{k} \cdot \mathbf{q}$. Here $\phi_k = \phi(k)$ is the quark gap angle related to the BCS angle θ_k by, $\tan(\phi_k - \theta_k) = m/k$, and $\omega_k = ke^{-2\theta_k}$ is the effective gluon self energy. The last term in Eq. (22) is due to the non-abelian component of the gluon kinetic energy. The quark gap equation is UV finite for the linear potential since $V_L(|\mathbf{p}|) = -8\pi\sigma/p^4$, but not for the Coulomb potential $V_C(|\mathbf{p}|) = -4\pi\alpha_s/p^2$. The gluon gap equation has both logarithmical and quadratical UV divergences and an integration cutoff, $\Lambda = 4$ GeV, determined in previous studies is used in both equations.

3 Applications

Predictions for the low-lying spectra of glueballs, hybrid mesons and tetraquark systems are now presented and discussed. Since these hadrons consist of 3 or more constituents, the masses for selected J^{PC} states are computed variationally

$$M_{J^{PC}} = \frac{\langle\Psi^{JPC}|H_{\text{eff}}|\Psi^{JPC}\rangle}{\langle\Psi^{JPC}|\Psi^{JPC}\rangle}. \quad (23)$$

The variational approximation has been comprehensively tested in two body systems by comparison with exact diagonalization and found to be accurate to a few percent.

3.1 Glueballs

Previous work [5] has investigated gg glueballs which only have $C = 1$. For $C = -1$ glueballs (oddballs), Fock states with at least 3 gluons are necessary and the variational wavefunction is ($\mathbf{q}_{i=1,2,3}$ are the cm gluon momenta)

$$|\Psi_{ggg}^{JPC}\rangle = \int d\mathbf{q}_1 d\mathbf{q}_2 d\mathbf{q}_3 \delta(\mathbf{q}_1 + \mathbf{q}_2 + \mathbf{q}_3) \quad (24)$$

$$\Phi_{\mu_1\mu_2\mu_3}^{JPC}(\mathbf{q}_1, \mathbf{q}_2, \mathbf{q}_3) C^{abc} \alpha_{\mu_1}^{a\dagger}(\mathbf{q}_1) \alpha_{\mu_2}^{b\dagger}(\mathbf{q}_2) \alpha_{\mu_3}^{c\dagger}(\mathbf{q}_3) |\Omega_{gluon}\rangle,$$

with color tensor C^{abc} either totally antisymmetric f^{abc} (for $C = 1$) or symmetric d^{abc} (for $C = -1$). Boson statistics thus requires the $C = -1$ oddballs to have a symmetric space-spin wavefunction. Using eq. (23) and a two-parameter variational radial wavefunction, the J^{--} oddball states have been calculated. Only the Abelian component of the magnetic fields are retained and the hyperfine interaction, H_{gg} , is suppressed. There are three terms contributing to the mass expectation value which are depicted in Fig. 1 which correspond to the gluon self-energy (top), gluon-gluon scattering (middle) and annihilation (bottom).

The nine-dimensional variational calculation was performed using the Monte Carlo method with the adaptive sampling algorithm VEGAS [9] and numerical convergence required between 10^5 and 10^6 samples. The oddball mass predictions are compared in Table 1 to available

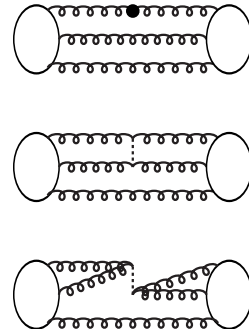


Fig. 1. Glueball diagrams for $\langle\Psi_{ggg}^{JPC}|H_{\text{eff}}|\Psi_{ggg}^{JPC}\rangle$.

Table 1. Glueball quantum numbers and masses in MeV. Error in H_{eff} (from Monte Carlo only) is 100 MeV or less, the quoted lattice errors are typically 200-300 MeV.

Model	1^{--}	3^{--}	5^{--}	7^{--}
Coulomb gauge H_{eff}	3950	4150	5050	5900
lattice [10]	3850	4130		
lattice [11]	3100	4150		
Wilson-loop [12]	3490	4030		

lattice gauge results [10,11] and a Wilson-loop inspired model [12]. A study of the glueball mass sensitivity to both statistical and variational uncertainties yielded error bars at the few per cent level.

Figure 2 displays predicted oddball Regge trajectories from the alternative approaches. Lattice results are depicted by open circles [10] and diamonds [11]. Constituent gluon predictions are represented by boxes, solid triangles and solid circles and correspond to a Wilson-loop inspired potential model [12], a simpler harmonic oscillator calculation [7] labeled H_M and the H_{eff} approach, respectively. The odderon trajectories for the latter two models are represented by the solid lines, $\alpha_O^M = 0.18t + 0.25$ and $\alpha_O^{\text{eff}} = 0.23t - 0.88$, which provide an overall theoretical uncertainty. The much steeper dashed line is the ω trajectory.

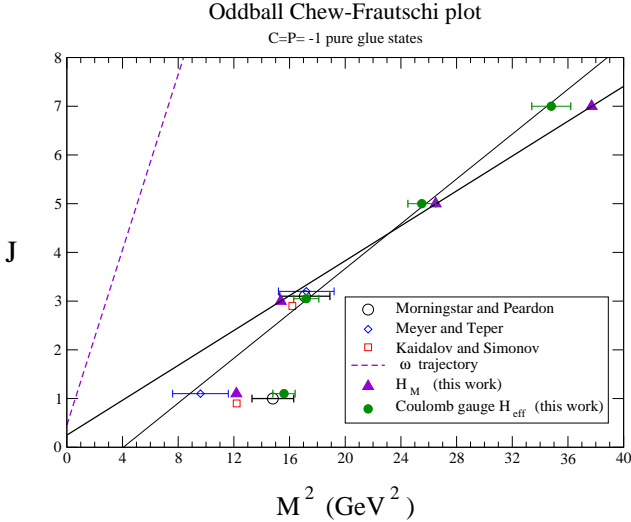


Fig. 2. Odderon trajectories from constituent gluon models and lattice compared to the ω meson Regge trajectory.

Three key results follow. First, the predicted odderon has slope similar to the pomeron but intercept clearly lower than the ω value. Second, the odderon starts with the 3^{--} state and not the 1^{--} which is on a daughter trajectory. Note that there are no lattice 5^{--} glueball predictions which are necessary to confirm this point and we strongly recommend that future studies calculate higher J^{--} states. Third, all approaches agree that the 3^{--} mass is near 4 GeV.

3.2 Hybrid mesons

We denote the momenta of the dressed quark, anti-quark and gluon by \mathbf{q} , $\bar{\mathbf{q}}$ and \mathbf{g} , respectively, and work in the hybrid cm system. The color structure for a $q\bar{q}g$ hybrid is given by $SU_c(3)$ algebra, $(3 \otimes \bar{3}) \otimes 8 = (8 \otimes 8) \oplus (8 \otimes 1) = 27 \oplus 10 \oplus 10 \oplus 8 \oplus 8 \oplus 1$. Hence for an overall color singlet the quarks must be in an octet state like the gluon which leads to a repulsive $q\bar{q}$ interaction, confirmed by lattice at short range, that raises the mass of the hybrid meson. The hybrid wavefunction has the general form

$$|\Psi_{q\bar{q}g}^{JPC}\rangle = \int d\mathbf{q} d\bar{\mathbf{q}} d\mathbf{g} \delta(\mathbf{q} + \bar{\mathbf{q}} + \mathbf{g}) \Phi_{\lambda\bar{\lambda}\mu}^{JPC}(\mathbf{q}, \bar{\mathbf{q}}, \mathbf{g}) T_{c\bar{c}}^a B_{\lambda c}^\dagger(\mathbf{q}) D_{\bar{\lambda} \bar{c}}^\dagger(\bar{\mathbf{q}}) \alpha_\mu^{a\dagger}(\mathbf{g}) |\Omega\rangle. \quad (25)$$

We have extended our previous hybrid study [3] by including the H_{qg} Hamiltonian term containing the $\mathbf{J}^a \cdot \mathbf{A}^a$ operators. Following [6], an effective quark hyperfine interaction with a $\mathbf{J}^a \cdot \mathbf{J}^a$ form is obtained using perturbation theory to second order in g and integrating over the gluonic degrees of freedom. This contribution to the hybrid mass is represented by the $q\bar{q}$ gluon exchange Feynman diagrams in Fig. 3 (first two in the bottom row). The non-abelian magnetic field terms are also included and entail triple-gluon vertices (last two diagrams in Fig. 3). The remaining diagrams represent the self-energy, scattering and quark annihilation mass contributions.

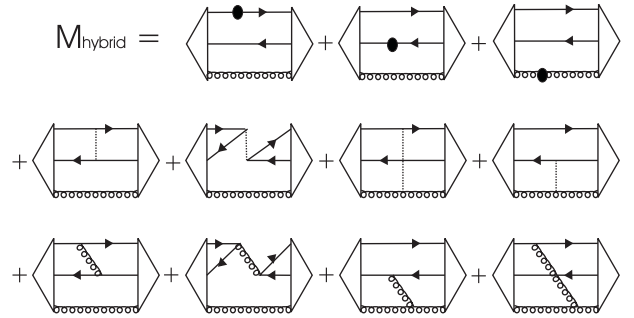


Fig. 3. Hybrid meson diagrams for $\langle \Psi_{q\bar{q}g}^{JPC} | H_{\text{eff}} | \Psi_{q\bar{q}g}^{JPC} \rangle$.

The hyperfine interaction from the H_{qg} term is

$$V_T = \frac{1}{2} \iint d\mathbf{x} d\mathbf{y} J_i^a(\mathbf{x}) \hat{U}_{ij}(\mathbf{x}, \mathbf{y}) J_j^a(\mathbf{y}), \quad (26)$$

with kernel reflecting the transverse gauge

$$\hat{U}_{ij}(\mathbf{x}, \mathbf{y}) = \left(\delta_{ij} - \frac{\nabla_i \nabla_j}{\nabla^2} \right)_{\mathbf{x}} \hat{U}(|\mathbf{x} - \mathbf{y}|). \quad (27)$$

The potential \hat{U} is a modified Yukawa with dynamical mass, $m_g = 600$ MeV, for the exchanged gluon as explained in [6]. Its momentum space representation is

$$U(p) = \begin{cases} -\frac{8.04}{p^2} \frac{\ln^{-0.62}(\frac{p^2}{m_g^2} + 0.82)}{\ln^{0.8}(\frac{p^2}{m_g^2} + 1.41)} & p > m_g \\ -\frac{24.50}{p^2 + m_g^2} & p < m_g \end{cases}. \quad (28)$$

The quark hyperfine interaction also generates additional terms in the quark gap equation [6].

The 12 dimensional integrals were calculated using the Monte Carlo method and repetitively evaluated with an increasing number of points until a weight-averaged result converged, typically involving about 50 million samples. The hybrid mass error introduced by this procedure is about ± 50 MeV. For each J^{PC} hybrid state we optimized the two variational parameters.

Using standard current quark masses, $m_u = m_d = 5$ MeV, $m_s = 80$ MeV and $m_c = 1000$ MeV, the predicted low-lying mass spectra for light and heavy hybrid mesons are presented in Figs. 4 and 5, respectively. Note that quark annihilation interactions increase the hybrid mass and this introduces isospin splitting since it only contributes in the $I_{q\bar{q}}$ channel. More importantly, all hybrid masses, especially the lightest exotic 1^{-+} state, are clearly above 2 GeV. This is consistent with lattice [13, 14, 15, 16, 17, 18, 19, 20] and Flux Tube model [21, 22, 23] results summarized in Table 2. These composite predictions strongly suggest that observed 1^{-+} $\pi(1600)$, and more clearly $\pi(1400)$, are not hybrid meson states.

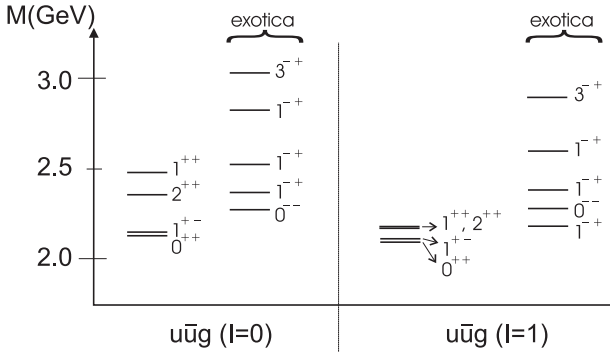


Fig. 4. Low lying $u\bar{u}g$ spectra.

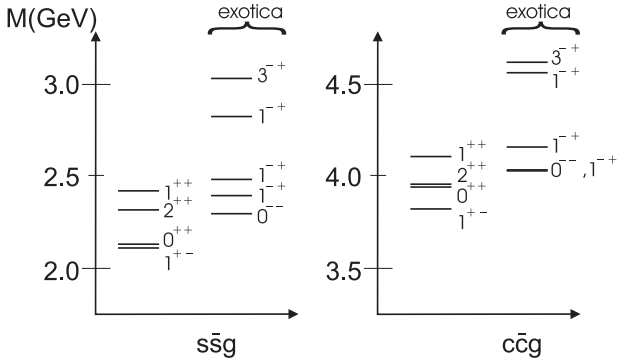


Fig. 5. Low lying $s\bar{s}g$ and $c\bar{c}g$ spectra.

The charmed $c\bar{c}g$ hybrid spectrum has a slightly different level order compared to the strange $s\bar{s}g$ and $u\bar{u}g$ spectra due to the hyperfine interaction. The predicted strange and charmed exotic 1^{-+} states are also in reasonable agreement with both lattice and Flux Tube results.

Table 2. Published predicted exotic 1^{-+} masses, in GeV, for light, strange and charmed hybrid mesons.

Model	u/d hybrid	s hybrid	c hybrid
Lattice QCD [13-20]	1.7 - 2.1	1.9	4.2 - 4.4
Flux Tube [21,22,23]	1.8 - 2.1	2.1 - 2.3	4.1 - 4.5

3.3 Tetraquark systems

This is the first four-body application using this approach. The $SU_c(3)$ color algebra for four quarks produces 81 color states, $3 \otimes 3 \otimes 3 \otimes 3 = 27 \oplus 10 \oplus \bar{10} \oplus 8 \oplus 8 \oplus 8 \oplus 1 \oplus 1$, of which two are color singlets that can be obtained in four different ways, depending on the intermediate color coupling: singlet scheme (molecule), octet scheme, and two diquark schemes involving the triplet and the sextet representations (see Fig. 6).

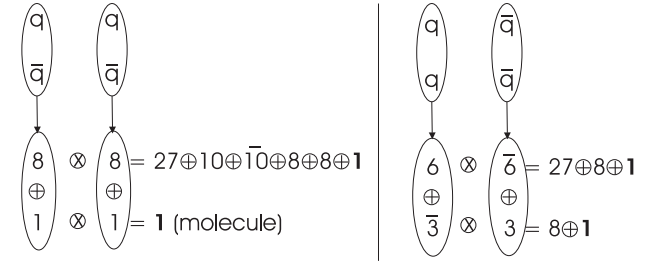


Fig. 6. Color singlets via four different representations.

Working in the cm system and denoting the momenta of the quarks by \mathbf{q}_1 and \mathbf{q}_3 , and those of the anti-quarks by \mathbf{q}_2 and \mathbf{q}_4 , the tetraquark wavefunction is

$$|\Psi_{4q}^{JPC}\rangle = \int d\mathbf{q}_1 d\mathbf{q}_2 d\mathbf{q}_3 d\mathbf{q}_4 \delta(\mathbf{q}_1 + \mathbf{q}_2 + \mathbf{q}_3 + \mathbf{q}_4) \Phi_{\lambda_1 \lambda_2 \lambda_3 \lambda_4}^{JPC}(\mathbf{q}_1, \mathbf{q}_2, \mathbf{q}_3, \mathbf{q}_4) R_{C_3 C_4}^{C_1 C_2} (29)$$

$$B_{\lambda_1 C_1}^\dagger(\mathbf{q}_1) D_{\lambda_2 C_2}^\dagger(\mathbf{q}_2) B_{\lambda_3 C_3}^\dagger(\mathbf{q}_3) D_{\lambda_4 C_4}^\dagger(\mathbf{q}_4) |\Omega_{quark}\rangle,$$

where the color elements $R_{C_3 C_4}^{C_1 C_2}$ depend on the specific color scheme chosen.

Contributions to the Hamiltonian expectation value are summarized in Fig. 7 and correspond to 4 self-energy, 6 scattering, 4 annihilation and 70 exchange terms each of which can be reduced to 12 dimensional integrals that are evaluated in momentum space. Because of the computationally intensive nature of this analysis, the hyperfine interaction was not included. Performing large-scale Monte Carlo calculations (typically 50 million samples), has conclusively determined that the molecular representation (i.e. meson-meson) produces the lightest mass state for a given J^{PC} . This is due to suppression of certain interactions (cancellation of color factors) in the singlet-singlet molecular representation and also the presence of repulsive forces in the other, more exotic, color schemes.

Using $m_u = m_d = 5$ MeV, the predicted tetraquark ground state is the non-exotic vector 1^{++} state in the molecular representation with mass around 1.2 GeV. Figures 8 and 9 depict the predicted tetraquark spectra for

References

1. A. P. Szczepaniak, E. S. Swanson, C. R. Ji and S. R. Cotanch, Phys. Rev. Lett. **76**, 2011 (1996).
2. F. J. Llanes-Estrada and S. R. Cotanch, Phys. Rev. Lett. **84**, 1102 (2000).
3. F. J. Llanes-Estrada and S. R. Cotanch, Phys. Lett. B **504**, 15 (2001).
4. F. J. Llanes-Estrada and S. R. Cotanch, Nucl. Phys. A **697**, 303 (2002).
5. F. J. Llanes-Estrada, S. R. Cotanch, P. Bicudo, J. E. Ribeiro and A. P. Szczepaniak, Nucl. Phys. A **710**, 45 (2002).
6. F. J. Llanes-Estrada, S. R. Cotanch, A. P. Szczepaniak and E. S. Swanson, Phys. Rev. C **70**, 035202 (2004).
7. F. J. Llanes-Estrada, P. Bicudo and S. R. Cotanch, Phys. Rev. Lett. **96**, 081601 (2006).
8. I. J. General, S. R. Cotanch and F. J. Llanes-Estrada, arXiv:hep-ph/0609115.
9. G. P. Lepage, Journal of Comput. Phys. **27**, 192 (1978); Cornell University Report CLNS 80-447, 1980 (unpublished).
10. C. J. Morningstar and M. Peardon, Phys. Rev. D **60**, 034509 (1999).
11. H. B. Meyer and M. Teper, Phys. Lett. B **605**, 344 (2005).
12. A. B. Kaidalov and Y. A. Simonov, Phys. Lett. B **477**, 163 (2000).
13. C. Bernard *et al.*, Phys. Rev. D **56**, 7039 (1997).
14. C. Bernard *et al.*, Nucl. Phys. (Proc. Suppl.) B **73**, 264 (1999).
15. P. Lacock and K. Schilling, Nucl. Phys. (Proc. Suppl.) B **73**, 261 (1999).
16. J. N. Hedditch *et al.*, Phys. Rev. D **72**, 114507 (2005).
17. X. Q. Luo and Z. H. Mei, Nucl. Phys. (Proc. Suppl.) B **119**, 263 (2003).
18. Y. Liu and X. Q. Luo, Phys. Rev. D **73**, 054510 (2006).
19. L. A. Griffiths, C. Michael and P. E. L. Rakow, Phys. Lett. B **129**, 351 (1983).
20. S. Perantonis and C. Michael, Nucl. Phys. B **347**, 854 (1990).
21. T. Barnes, F. E. Close and E. S. Swanson, Phys. Rev. D **52**, 5242 (1995).
22. F. E. Close and P. R. Page, Nucl. Phys. B **443**, 233 (1995).
23. K. Waidelich, Diploma Thesis, North Carolina State University (2001).
24. E. R. Berger, *et al.*, Eur. Phys. J. C **9**, 491 (1999).
25. E. R. Berger, *et al.*, Eur. Phys. J. C **14**, 673 (2000).
26. A. P. Szczepaniak and P. Krupinski, Phys. Rev. D **73**, 116002 (2006).